Universal infrared absorbance of two-dimensional honeycomb group-IV crystals

Lars Matthes,[1,2] Paola Gori,[3] Olivia Pulci,[2] and Friedhelm Bechstedt[1]

[1]*Institut für Festkörpertheorie und -optik, Friedrich-Schiller-Universität, Max-Wien-Platz 1, 07743 Jena, Germany*

[2]*ETSF and Dipartimento di Fisica, Università di Roma Tor Vergata, Via della Ricerca Scientifica 1, I-00133 Rome, Italy*

[3]*ETSF and CNR-ISM, Via Fosso del Cavaliere 100, I-00133 Rome, Italy*

(Received 26 June 2012; revised manuscript received 15 January 2013; published 31 January 2013)

We show that the low-frequency absorbance of undoped graphene, silicene, and germanene has a universal value, only determined by the Sommerfeld fine-structure constant. This result is derived by means of *ab initio* calculations of the complex dielectric function for optical interband transitions applied to two-dimensional (2D) crystals with honeycomb geometry. The assumption of chiral massless Dirac fermions is not necessary. The low-frequency absorbance does not depend on the group-IV atom, neither on the sheet buckling nor on the orbital hybridization. We explain these findings via an analytical derivation of the relationship between absorbance and fine-structure constant for 2D Bloch electrons. The effect of deviations of the electronic bands from linearity is also discussed.

DOI: 10.1103/PhysRevB.87.035438 PACS number(s): 73.22.Pr, 78.20.−e, 78.67.−n, 78.67.Wj

I. INTRODUCTION

The two-dimensional (2D) material graphene with its honeycomb crystal structure, the characteristic π bonding, and its peculiar band structure[1] has lead to the discovery of chiral massless charge carriers, the Dirac fermions.[2,3] Among the unique properties of graphene, the optical ones are of special interest. A constant infrared dynamic conductivity and optical absorbance have been predicted and also measured.[4–8] It has also been demonstrated experimentally that visual transparency of graphene is only determined by the Sommerfeld fine-structure constant $\alpha = 1/137.036$:[6,7] because of Dirac cones in the 2D band structure of graphene, its opacity or absorbance is given by $\pi\alpha$ in the low-frequency limit. This result has been obtained by means of the theory of noninteracting isotropic Dirac fermions with pseudospin and using the vector-potential gauge for the electromagnetic field (see Refs. 6,9–11 and references therein). Recently, also an effective fine-structure constant of freestanding graphene has been measured in graphite.[12]

The question then arises if other 2D honeycomb crystals based on group-IV elements could present the same remarkable absorption feature at low frequency. *Ab initio* theory predicts the stability of graphene-like 2D hexagonal silicon, called silicene, and germanium, the so-called germanene.[13] Differently from graphene, the Si- and Ge-based crystals are buckled and do not show an sp^2 hybridization but instead a mixed $sp^2 - sp^3$ one. Despite a resulting buckling amplitude Δ, the π and σ bands are still decoupled in silicene and germanene, and Dirac cones are formed by the π and π^* bands[14] with zero gap at the corners K and K' of the 2D Brillouin zone, although with a different slope and therefore Fermi velocity compared to graphene. Interesting properties have also been recently predicted for 2D honeycomb crystals of silicon carbide,[15] which, however, possess a large direct gap at K and K' due to the symmetry breaking of the two sublattices and the consequent charge transfer between Si and C atoms. Hence, no Dirac cones are present in the electronic structure of SiC layers. A gap is also opened and Dirac cones are destroyed when hydrogenation leads to a full sp^3 hybridization of the 2D group-IV crystals.[16]

Very recently, the existence of silicene has been experimentally demonstrated, at least in form of epitaxial sheets[17,18] and nanoribbons[19,20] on silver surfaces and on diboride thin films.[21] Apart from *ab initio* studies of the absorbance for vanishing frequencies in a brief letter,[22] neither theoretical predictions nor measurements of the optical properties of silicene and germanene are available.

In this paper, we study if the direct relation of the absorbance to the fine-structure constant remains conserved in the presence of real-structure effects such as the actual Fermi velocity of the Dirac fermions and anisotropic deviations from the linear wave-vector dispersion around the K and K' Dirac points. The influence of the incomplete sp^2 hybridization and hence of the buckling of the honeycomb lattice is investigated in the case of silicene and germanene. The effect of the gauge of the electromagnetic field is discussed for vanishing photon wave vectors. All issues are investigated using both *ab initio* and analytic calculations of the dielectric function. Self-energy and excitonic effects due to the electron-electron interaction[8,23] in the sheet crystals are not taken into account.

The physical approaches and numerical methods are described in Sec. II. Results of first-principles computations including full band structures and analytical calculations for Dirac particles are presented in Sec. III. Finally, in Sec. IV, a brief summary and conclusions are given.

II. APPROACHES AND COMPUTATIONAL METHODS

A. Atomic structure and electronic states

Our calculations of the ground-state, electronic and optical properties are based on the density functional theory (DFT)[24,25] as implemented in the Vienna *ab initio* simulation package (VASP).[26,27] Exchange and correlation (XC) are described within the generalized gradient approximation (GGA).[28,29] Pseudopotentials for C$1s^2$, Si$1s^2 2s^2 2p^6$, and Ge$1s^2 2s^2 2p^2 3s^2 3p^6 3d^{10}$ cores and all-electron-like wave functions are generated within the projector-augmented wave (PAW) method.[30,31] The wave functions between the cores are expanded in plane waves with a kinetic energy cutoff of 500 eV. The isolated C, Si, and Ge honeycomb layers

TABLE I. Lattice constant a and buckling amplitude Δ for group-IV honeycomb crystals. The Fermi velocity v_F is also listed.

	C	Si	Ge
a (Å)	2.466	3.866	4.055
Δ (Å)	0.00	0.45	0.69
v_F (10^6 m/s)	0.829	0.532	0.517

are simulated by a graphite-like superlattice arrangement with a large superlattice period, i.e., a distance between two adjacent layers of $L = 20$ Å. The integration over the flat and, hence, two-dimensional Brillouin zone (BZ) is replaced by a Γ-centered $64 \times 64 \times 1$ **k**-point Monkhorst-Pack[32] mesh.

In the electronic-structure and optical studies, self-energy and excitonic effects are not taken into account. It has been shown for graphene that in the energy range below 2 eV, where the approximation of Dirac particles is valid, the influence of the many-particle effects is negligible.[8] At the Dirac points, the quasiparticle effects vanish. Moreover, we will show that the zero-frequency result is independent of the absolute value of the Fermi velocity v_F. Its renormalization by self-energy effects[8] is therefore not expected to affect the low-frequency result. The Fermi velocities in Table I represent values that are only slightly smaller than the velocity measured for graphene.[3] For silicene on silver substrates, a larger v_F value is measured[17] especially because of the influence of the metal. Of course, for higher photon energies in the range of the interband critical points, the many-body effects will influence the optical spectra. Nevertheless, in this energy region, a partial compensation of quasiparticle and excitonic effects takes place. While the quasiparticle self-energy effects give rise to a blue shift of the transition energies, the screened attraction of electrons and holes leads to a redshift. Consequently, the Kohn-Sham eigenvalues and eigenfunctions[25] are used in all numerical calculations.

In general, the influence of the electron-electron interaction on the optical polarization function, i.e., on its irreducible part, in graphene is controversially discussed in the literature, especially in the low-frequency limit. First-order perturbation theory including self-energy and ladder diagrams seems to give renormalizations in the order of percent (see Ref. 23 and references therein). One result is the logarithmic renormalization of the Fermi velocity. However, such logarithmic divergences cannot be resumed in higher-order perturbation theory, and also angle-resolved photoemission spectroscopy of graphene does not show any evidence (see Ref. 33 and references therein). The situation seems to be similar for silicene and germanene. Despite their sheet buckling and the partial sp^3 bonding, the electronic states near the Dirac points are still dominated by π states. For wave vectors near the corner points of the BZ, the π and σ states are still decoupled because of the point symmetry of the honeycomb lattice.[14] The difference to graphene is, however, that massless Dirac-Weyl fermions only appear in smaller energy intervals around the zero gap.[22] Another important point is that spin-orbit interaction becomes important. Especially for germanene with a corresponding gap opening of about 24 meV,[34] it seems to be more important in the $\omega \to 0$ limit than the electron-electron interaction being marginally irrelevant near the Dirac points.[33]

We focus in this work on undoped materials, and therefore we neglect electron-plasmon interaction that was recently shown to be promisingly exploitable for plasmonics using doped graphene.[35] The deviations from a constant absorbance of graphene for measurements down to photon energies of 0.2 eV[7] may indeed be reduced to a Drude behavior of free carriers. However, here, no Fermi-level position in Dirac cones is investigated. Consequently, band filling effects, which are described by the Burstein-Moss shift in semiconductors with finite gap[36] are also not taken into account. Another source of departure from the universal value of absorbance in the far-infrared region is due to intraband transitions caused by scattering with phonons.[37] However, a direct absorption of light by phonons is impossible since lattice vibrations in graphene, silicene, and germanene do not span dynamical dipoles. Therefore free carrier and phonon contributions do not play a role in agreement with the experimental findings for several samples (see, e.g., Nair *et al.*[6]). Here, we have only to deal with the consequences of interband transitions for the three studied 2D honeycomb crystals.

B. Frequency-dependent dielectric function

The optical properties of the 2D crystals are derived from the in-plane dielectric function $\epsilon(\omega)$ for normal incidence in the independent-particle approximation[38] for the used superlattice arrangement. Here, we only study undoped 2D group-IV crystals where the Fermi energy crosses the zero gap. Therefore, in the low-temperature limit, only optical interband transitions take place. The electrons and holes are described as common fermions. The Bloch bands $\varepsilon_\nu(\mathbf{k})$ with their full wave-vector dispersion are taken into account. The optical absorption is determined by the imaginary part of the dielectric function written in form of the Ehrenreich-Cohen formula for completely empty conduction (filled valence) bands $\nu = c$ ($\nu = v$):

$$\epsilon(\omega) = 1 + \frac{8\pi}{L\,A} \sum_{c,v} \sum_{\mathbf{k}} |M_{cv}(\mathbf{k})|^2 \times \sum_{\beta=\pm} \frac{1}{\varepsilon_c(\mathbf{k}) - \varepsilon_v(\mathbf{k}) + \beta(\hbar\omega + i\gamma)} \tag{1}$$

with A as the sheet area and L the distance between the sheets in the periodic supercell arrangement. Within the longitudinal approach,[39] the optical transition matrix element is given by

$$M_{cv}(\mathbf{k}) = \lim_{\mathbf{q}\to 0} \tfrac{e}{|\mathbf{q}|} \langle c;\mathbf{k}|e^{i\mathbf{q}\cdot\mathbf{r}}|v;\mathbf{k}+\mathbf{q}\rangle \tag{2}$$

for a vanishing vector $\mathbf{q}$ (whose direction is later identified with that of light polarization) with the Bloch functions $|\nu;\mathbf{k}\rangle$ ($\nu = c,v$; $\mathbf{k} \in$ BZ).

Within the PAW approach, these functions are all-electron wave functions. The corresponding Hamiltonian is local in space and, hence, the dipole matrix element can be directly related to the optical transition matrix element of the momentum operator $\mathbf{p}$, since the commutator of the Hamiltonian and the space operator is related to the momentum operator $\mathbf{p}$.[38] Equation (2) can be rewritten as

$$M_{cv}(\mathbf{k}) = \frac{e\hbar}{m} \frac{\langle c;\mathbf{k}|\frac{\mathbf{q}}{|\mathbf{q}|}\mathbf{p}|v;\mathbf{k}\rangle}{\varepsilon_c(\mathbf{k}) - \varepsilon_v(\mathbf{k})}. \tag{3}$$

The appearance of the momentum-operator matrix element can be also interpreted as the use of the transverse gauge of the electromagnetic field. Varying the orientation of the photon wave vector $\mathbf{q}$, the full dielectric tensor can be determined.[39] Here, only in-plane wave vectors are considered.

Sometimes the two different types of optical transition matrix elements in Eqs. (2) and (3) are identified as the consequence of different, longitudinal and transverse, gauges of the electromagnetic field.[39] This is in agreement with the fact that for macroscopically isotropic systems (such as a sheet with hexagonal symmetry) the longitudinal and transverse in-plane dielectric functions are identical in the limit of vanishing photon wave vectors.

The frequency-dependent electronic polarizability of an isolated sheet can be derived from Eq. (1) by

$$\alpha(\omega) = L[\epsilon(\omega) - 1]/4\pi. \tag{4}$$

The optical absorption in an isolated sheet is given by the imaginary part of the 2D electronic polarizability $\mathrm{Im}\alpha(\omega) = L\,\mathrm{Im}[\epsilon(\omega) - 1]/4\pi = L\,\mathrm{Im}\epsilon(\omega)/4\pi$, which is directly related to the thickness-independent absorbance of such a sheet $A(\omega) = \frac{4\pi\omega}{c}\mathrm{Im}\alpha(\omega)$, i.e.,

$$A(\omega) = \frac{\omega}{c} L\,\mathrm{Im}\epsilon(\omega) \tag{5}$$

with c as the speed of light. We have calculated $A(\omega)$ and the optical spectra using a refined Monkhorst-Pack mesh of $400 \times 400 \times 1$ $\mathbf{k}$ points. A total of 16 bands is taken into account. The low-energy limit of the absorbance is calculated using a further refined, nonuniform hybrid mesh of $\mathbf{k}$ points around K (or K') BZ boundary points (about 13 700 mesh points) in a sector corresponding to the irreducible part with a radius $0.05\ 2\pi/a$.

III. RESULTS AND DISCUSSION

A. Geometry and electronic structure

The optimized atomic geometries have been obtained by minimizing the total energy as a function of the lateral lattice parameter a. At each value of the lattice constant a, the atomic positions, for symmetry reasons, essentially the sheet buckling Δ, were fully relaxed to reduce the Hellmann-Feynman forces to values below 1 meV/Å. Results are summarized in Table I. In the carbon case, the optimized lattice is unbuckled ($\Delta = 0$), whereas the minimum of the total energy with a finite buckling $\Delta = 0.45$ Å is lower in energy for silicene. For germanene, only the buckled structure is stable with $\Delta = 0.69$ Å. For silicene and germanene, the optimized buckling amplitudes are slightly smaller than the value $\Delta = a/2\sqrt{6}$ predicted for a complete sp^3 hybridization. Together with the buckling amplitudes, the resulting lattice constants $a = 2.47$ Å (graphene), 3.87 Å (silicene), and 4.06 Å (germanene) in Table I follow a clear chemical trend.

In general, our structural results are in agreement with previous DFT calculations.[13,40–43] In any case, the sheet buckling in silicene and germanene exhibits strong deviations from the sp^2 hybridization of planar graphene toward an sp^3 hybridization similarly to bulk Si and Ge crystallizing in diamond structure. The deviations from the planar geometry and the sp^2 bonding are usually important for avoiding a metallic character of the 2D honeycomb crystals, in particular in the Ge case.[44] Nevertheless, despite the buckling, the π and σ bands remain decoupled in silicene and germanene for symmetry reasons[13] with the resulting gap to be zero as for graphene.

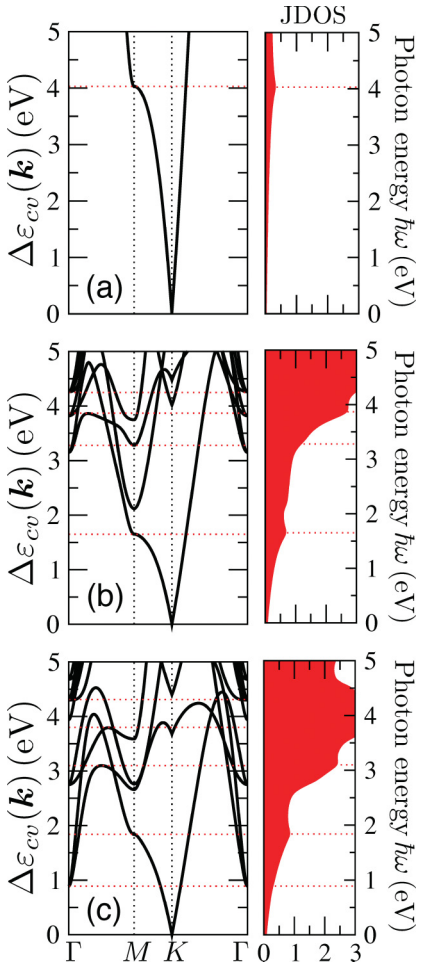

FIG. 1. (Color online) Interband transition energies along high-symmetry lines in the BZ for graphene (a), silicene (b), and germanene (c). The red horizontal lines indicate energies of van Hove singularities which give peak structures in the absorbance in Figs. 2 and 5. The resulting joint densities of states $D(\omega)$ are displayed in addition [in units of $(\mathrm{eV})^{-1}$].

The eigenvalues $\varepsilon_v(\mathbf{k})$ of the Kohn-Sham equation[25] are used to illustrate the optical interband transition energies $\Delta\varepsilon_{cv}(\mathbf{k}) = \varepsilon_c(\mathbf{k}) - \varepsilon_v(\mathbf{k})$ and the joint density of states (JDOS) $D(\omega)$. Results for three honeycomb sheet materials are given in Fig. 1. They illustrate how and with which joint density of states the energy conservation is fulfilled in the optical absorption for a given photon energy $\hbar\omega$. In the range of very low photon energies, whose limit decreases along the row C, Si, and Ge, the isotropic Dirac cones are also visible in the joint band structure at K (or K'). The Dirac cones give rise to a linear increase of $D(\omega)$ in the low-energy region $\hbar\omega$. For higher interband energies, the critical points $\mathbf{k}_0$ and van Hove singularities $\nabla_{\mathbf{k}}[\varepsilon_c(\mathbf{k}) - \varepsilon_v(\mathbf{k})]|_{\mathbf{k}=\mathbf{k}_0} = 0$ appear. Their energies are indicated by horizontal lines in the interband structure. They indeed give rise to spectral features in the JDOS $D(\omega)$ beginning near 4.0 eV (graphene), 1.6 eV (silicene), and

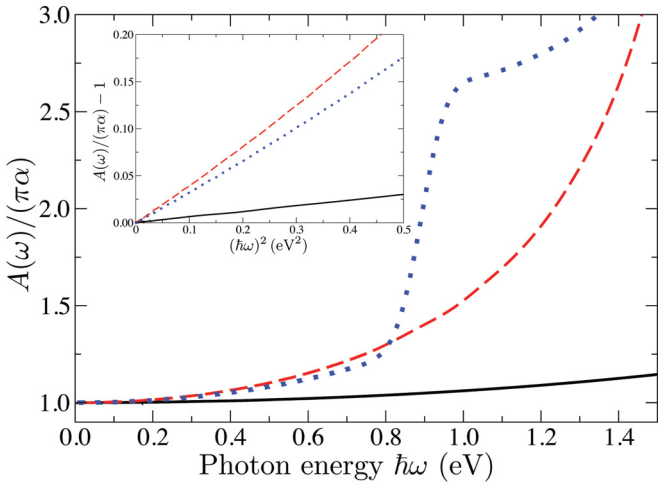

FIG. 2. (Color online) *Ab initio* calculated optical absorbance of graphene (black solid line), silicene (red dashed line), and germanene (blue dotted line) *vs* photon energy. The absorbance is normalized to $\pi\alpha$. The reduced infrared absorbance is depicted in the inset vs photon-energy square.

0.9 eV (germanene). The weak intensity of the lowest van Hove singularity for germanene at 0.9 eV related to the lowest interband transition at Γ is due to its small effective interband mass. Division of $D(\omega)$ by $\hbar\omega$ makes this van Hove singularity visible in the absorbance spectrum of germanene (see Fig. 2).

B. Low-frequency absorbance

The frequency dependence of the absorbance (5) is calculated numerically from Eq. (1) for the dielectric function using the *ab initio* electronic structure, more precisely the band structure $\varepsilon_v(\mathbf{k})$ and Bloch functions $|v;\mathbf{k}\rangle$. The obtained interband structures are plotted in Fig. 1 in a small range of photon energies for the three studied 2D crystals. The longitudinal representation[39] of the optical transition matrix elements (2) has been used. First, we investigate the resulting infrared absorbance as displayed in Fig. 2. Indeed, for graphene, we observe the result, known from measurements[6,7] and from the theoretical prediction assuming Dirac fermions and the vector-potential (transverse) gauge,[6] that in the limit $\omega \to 0$, the absorbance approaches to $A(0) = \pi\alpha$ (=0.022925) with $\alpha = e^2/\hbar c$ in excellent agreement with the predicted value and also in good agreement with the experimental findings for practically undoped graphene.[7,8] We find that this holds also for silicene and germanene and that the numerical values are $A(0) = 0.02293$ (graphene), 0.02290 (silicene), and 0.02292 (germanene). Hence the absorbance $A(0)$ is independent of the studied group-IV material and of the sheet buckling, i.e., of the strong deviations from the sp^2 hybridization in silicene and germanene. The reason is that the point-group symmetry of a 2D honeycomb lattice is conserved independent of the buckling amount.

The result in Fig. 2 has been found within a (normal) Fermi-liquid approximation with optical interband transitions between occupied and empty Bloch states. Important ingredients are of course the linear $\mathbf{k}$ dispersion of interband energies $\Delta\varepsilon_{cv}(\mathbf{k}) = \varepsilon_c(\mathbf{k}) - \varepsilon_v(\mathbf{k})$ (see Fig. 1) for extremely small photon energies and precise values of the optical matrix elements between pure π and π^* bands at the corner points of the BZ, $\mathbf{k} \hat{=} K$ or K', independent of the 2D material.

C. Matrix elements

The matrix elements for the lowest interband transitions between the highest valence band v and the lowest conduction band c are plotted in Fig. 3(a) along three high-symmetry lines including the BZ boundary KM (or $K'M$). For comparison, the corresponding π and π^* bands, that are involved in the optical transitions, are shown in Fig. 3(b). Of course, away from the BZ boundary near K or K' the first σ and σ^* bands along the ΓM line and in its vicinity appear for silicene and germanene close to the π and π^* bands. In Fig. 3, the band energies and the momentum matrix elements are normalized to their characteristic values $\hbar v_F\pi/a$ and $m^2v_F^2$, respectively, in the Dirac-Weyl theory, i.e., near K (or K'), in order to demonstrate that in the studied energy and wave-vector regions they are rather independent of the material.

Most important for the result $A(0) = \pi\alpha$ are the finite interband transition matrix elements around K (or K') in

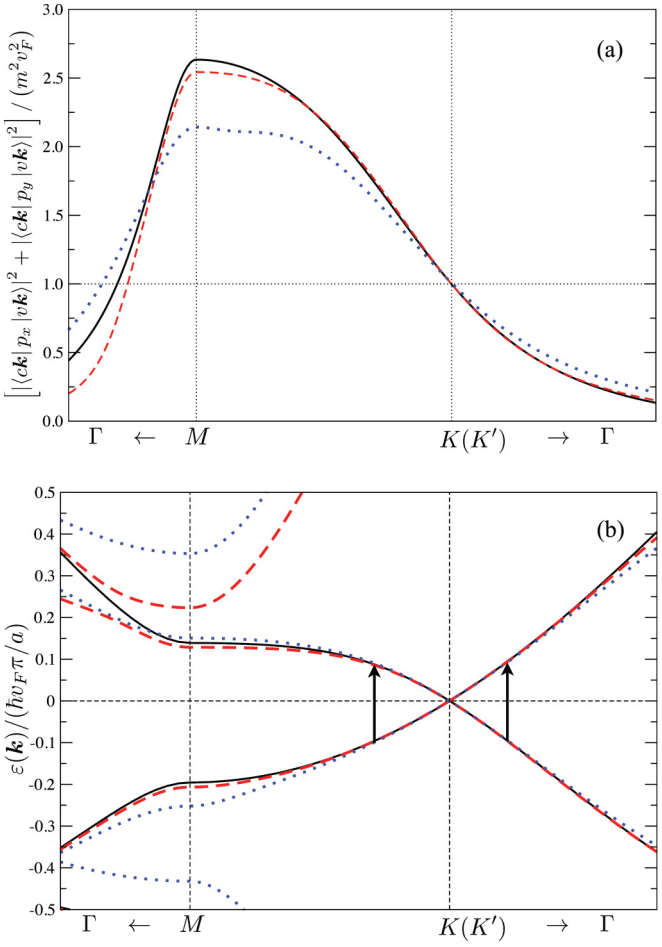

FIG. 3. (Color online) (a) Transition matrix elements of the pure $\pi - \pi^*$ transitions along high-symmetry lines in the BZ for graphene (black solid line), silicene (red dashed line), and germanene (blue dotted line). The longitudinal representation (2) has been used in the numerical calculations. (b) For illustration, the π and π^* bands that are involved in the optical transitions are also shown, indicated by vertical arrows.

Fig. 3(a). For their explicit computation, the longitudinal representation (2) has been used. The results presented in Fig. 3(a) are, however, rewritten as the momentum matrix elements according to the relation between Eqs. (2) and (3). They indicate that for low photon energies the optical properties, which according to the interband structure and the joint density of states are due to $\pi \to \pi^*$ transitions, are dominated by contributions from $\mathbf{k}$ points near the BZ boundary along the MK (or MK') lines. The matrix elements possess a maximum at an M point where, however, the underlying atomic symmetry of the wave functions is modified with respect to that at a K or K' point. The effects of the group-IV material and the sheet buckling are small. More precisely, at K and K' the momentum matrix-element squares are the same in units of $(mv_F)^2$. Indeed, the numerical treatments yield to values 0.995 (graphene), 0.995 (silicene), and 1.004 (germanene) very close to the value 1 (see below) expected. The numbers also illustrate the quality of the PAW functions used for the calculation of optical properties.[38] In general, the normalized momentum matrix element appearing in Fig. 3(a) only exhibits a weak wave-vector dispersion. At M, a minor reduction occurs along the row C $\to$ Si $\to$ Ge, whereas along $K\Gamma$ and $M\Gamma$ an opposite tendency is observed. The chemical trends are in rough agreement with the energy differences of the π and π^* bands in Fig. 3(b). Along KM, the interband energies are increased, while they are slightly reduced from K toward Γ.

D. Understanding within an analytical approach

The result $A(0) = \pi\alpha$ can be also analytically derived, using the tight-binding method[14,45] but restricting only to the p_z-orbitals and their nearest-neighbor interaction. Inserting Eq. (1) into Eq. (5), for normal incidence, and, thus, in-plane polarization of the light, the optical absorbance of a two-dimensional crystal is described by

$$A(\omega) = \frac{8\pi^2\omega}{cA}\sum_{c,v}\sum_{\mathbf{k}}|M_{cv}(\mathbf{k})|^2\delta[\varepsilon_c(\mathbf{k}) - \varepsilon_v(\mathbf{k}) - \hbar\omega], \quad (6)$$

where all interband transitions between Bloch states $|v;\mathbf{k}\rangle$ with energy $\varepsilon_v(\mathbf{k})$ and $|c;\mathbf{k}\rangle$ with energy $\varepsilon_c(\mathbf{k})$ are taken into account. Within the transverse gauge, the transition matrix elements $M_{cv}(\mathbf{k})$ (3) are directly related to the momentum matrix elements $\langle c;\mathbf{k}|p_x|v;\mathbf{k}\rangle$ and $\langle c;\mathbf{k}|p_y|v;\mathbf{k}\rangle$ of the in-plane momentum operator.

In the limit of vanishing frequencies $\omega \to 0$, only the lowest π^*-like conduction band $c = +$ and the highest π-like valence band $v = -$ near K and K' points contribute to the interband absorption (cf. Fig. 1). For symmetry reasons, honeycomb crystals are optically isotropic for normal incidence. Together with the replacement of the wave-vector sum in Eq. (6) by an integral over the BZ one finds

$$A(\omega) = \frac{\alpha\hbar}{m^2\omega}\int_{\mathrm{BZ}} d^2\mathbf{k}\sum_{j=x,y}|\langle +;\mathbf{k}|p_j|-;\mathbf{k}\rangle|^2 \times \delta[\varepsilon_+(\mathbf{k}) - \varepsilon_-(\mathbf{k}) - \hbar\omega], \quad (7)$$

where the Sommerfeld fine-structure constant α has been introduced. The two bands of the lowest interband pair of the studied 2D zero-gap semiconductors form Dirac cones at the three K and three K' points $\mathbf{k}_{oi}$ $(i = 1-6)$ (see Fig. 1). Because of the energy conservation in Eq. (6) we restrict the $\mathbf{k}$ integral to these six important regions in the BZ from which the principal contributions to the optical absorption are expected for low photon energies. Thereby, we have to take in mind that groups of three K (K') points are equivalent and only one third of each environment of a K (K') point belongs to the BZ. So we have in total to study only two nonequivalent $\mathbf{k}_{oi}$ (one K and one K') points with their full environment. Because of the convergence of all integrals we extend these environments to infinite.

The bands in Fig. 3(b) forming the Dirac cones at each $\mathbf{k}_{oi}$ are

$$\varepsilon_\pm(\mathbf{k}_{oi} + \Delta\mathbf{k}) = \pm\hbar v_F|\Delta\mathbf{k}| \quad (8)$$

with $\Delta\mathbf{k} = \mathbf{k} - \mathbf{k}_{oi}$. The Fermi velocity v_F in Table I characterizes the linear band dispersion. Then, Eqs. (7) and (8) give rise to

$$A(\omega) = \frac{\alpha\hbar}{m^2\omega}\sum_{i=1}^{2}\sum_{j=x,y}\int d^2(\Delta\mathbf{k}) \times |\langle +;\mathbf{k}_{oi} + \Delta\mathbf{k}|p_j|-;\mathbf{k}_{oi} + \Delta\mathbf{k}\rangle|^2 \times \delta(2\hbar v_F|\Delta\mathbf{k}| - \hbar\omega). \quad (9)$$

The strength of the optical transitions between the Dirac cones of electrons and holes is determined by the squares of the momentum matrix elements between the valence band $v = -$ and the conduction band $c = +$ [see Fig. 3(a)]. We investigate them near a K (or K') point $\mathbf{k}_{oi}$. We assume [and indeed we numerically found in Fig. 3(a)] that the transitions, despite their vanishing excitation energy, are dipole-allowed at $\mathbf{k} = \mathbf{k}_{oi}$. Their strength is given by $D = \sum_{j=x,y}|\langle +;\mathbf{k}_{oi}|p_j|-;\mathbf{k}_{oi}\rangle|^2$. At such a Dirac point $\mathbf{k}_{oi}$, in the limit $\Delta\mathbf{k} \to 0$, the two Bloch functions $|+;\mathbf{k}_{oi}\rangle$ and $|-;\mathbf{k}_{oi}\rangle$ approach to each other (apart from a phase factor). This is shown in Fig. 4 where the squared moduli of the eigenstates are depicted for silicene. The squares are identical for the lowest unoccupied state

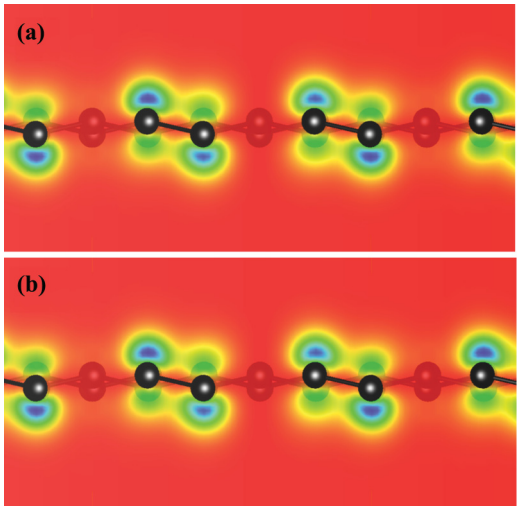

FIG. 4. (Color online) Wave-function squares in silicene for the highest occupied π state (a) and the lowest unoccupied π^* state (b) at K. The atomic positions in the isolated Si sheet indicate the buckled honeycomb geometry.

and the highest occupied state as well as for K and K' (not shown). Their symmetry and the maxima to find an electron or hole are identical. This can also be immediately seen using a tight-binding approximation with p_z orbitals localized at A and B atoms.[14] Consequently, at K or K', the strength can be approximately replaced by $D = \sum_{j=x,y} |\langle \pm; \mathbf{k}_{oi}|p_j|\pm; \mathbf{k}_{oi}\rangle|^2$, i.e., formally by intraband transition matrix elements. For intraband matrix elements, it however holds $\langle \nu; \mathbf{k}|\mathbf{p}|\nu; \mathbf{k}\rangle = \frac{m}{\hbar}\nabla_{\mathbf{k}}\varepsilon_\nu(\mathbf{k})$. Together with Eq. (8) then the total strength is found to be

$$D = (mv_F)^2 \tag{10}$$

in complete agreement with the *ab initio* calculations in Fig. 3(a). This result also follows within the nearest-neighbor tight-binding approximation if the parameter M as defined by Grüneis *et al.*[14] is related to the Fermi velocity as $|M| = \sqrt{\frac{8}{3}}mv_F$.

With the value (10) of the momentum matrix elements at a K or K' point it follows from Eq. (9) in the vanishing frequency limit,

$$A(\omega) = 2\frac{\hbar v_F^2}{\omega}\alpha \int d^2(\Delta\mathbf{k})\delta(2\hbar v_F|\Delta\mathbf{k}| - \hbar\omega). \tag{11}$$

Interestingly, similar integrals appear in a time-dependent formulation of the response of Dirac-Weyl particles.[11] Finally, we obtain

$$A(\omega) = 2\frac{\hbar v_F^2}{\omega}\alpha\frac{\pi\omega}{2\hbar v_F^2} = \pi\alpha. \tag{12}$$

In the limit of vanishing optical transition energies, the crystal-material dependence in the matrix elements and that in the interband energies compensate each other. Indeed, the infrared absorbance is determined by a universal constant, the Sommerfeld fine-structure constant for all honeycomb crystals formed by only one group-IV element.

E. Corrections to the infrared absorbance for $\omega > 0$

In order to obtain an analytical result that remains valid also for $\omega > 0$, we improve the band dispersion, more precisely, take deviations from the isotropic Dirac cones into account, but also account for the wave-vector dispersion of the transition matrix elements away from the Dirac points K and K'. In the tight-binding approximation with first nearest-neighbor interaction, one finds instead of $\epsilon_+(\mathbf{k}) - \epsilon_-(\mathbf{k}) = 2\hbar v_F|\Delta\mathbf{k}|$ in Eqs. (8) and (9) the corrected $\pi - \pi^*$ interband energies

$$\epsilon_+(\mathbf{k}) - \epsilon_-(\mathbf{k}) = 2\hbar v_F\frac{2}{\sqrt{3}a}|f(\mathbf{k})| \tag{13}$$

with the structure factor

$$f(\mathbf{k}) = \exp\left(i\frac{\sqrt{3}a}{2}k_x\right) + 2\cos\left(\frac{a}{2}k_y\right). \tag{14}$$

Correspondingly, the optical matrix elements are given by

$$\langle +; \mathbf{k}|p_j|-; \mathbf{k}\rangle = \frac{mv_F}{\sqrt{3}a}\frac{2i}{|f(\mathbf{k})|}Im\left[f^*(\mathbf{k})\frac{\partial}{\partial k_j}f(\mathbf{k})\right]. \tag{15}$$

For the K- and K'-point contributions to Eq. (9), we expand Eqs. (13) and (15) to the second order in the wave-vector deviation $\Delta\mathbf{k}$ from such a high-symmetry point. It means that the nonlinearity and anisotropy of the interband Dirac cones as illustrated in Fig. 1 are taken into account,[46]

$$\epsilon_+(\mathbf{k}) - \epsilon_-(\mathbf{k}) = 2\hbar v_F|\Delta\mathbf{k}|\left[1 \pm \frac{a}{4\sqrt{3}}\sin(3\varphi)|\Delta\mathbf{k}|\right]. \tag{16}$$

In addition, also the anisotropic wave-vector dispersion of the matrix elements in Fig. 3(a) contributes according to

$$\sum_{j=x,y}|\langle +; \mathbf{k}|p_j|-; \mathbf{k}\rangle|^2 = m^2v_F^2\left[1 \pm \frac{a}{\sqrt{3}}\sin(3\varphi)|\Delta\mathbf{k}| + \frac{1}{6}a^2\cos^2(3\varphi)|\Delta\mathbf{k}|^2\right]. \tag{17}$$

As a result of integration of Eq. (9) using the polar coordinates $|\Delta\mathbf{k}|$ and φ, we obtain the first nonvanishing frequency-dependent correction to the absorbance according to

$$A(\omega) = \pi\alpha[1 + \beta^2(\hbar\omega)^2] \tag{18}$$

with $\beta = \frac{\sqrt{3}a}{8\hbar v_F}$. This result indicates a parabolic deviation with respect to ω from the zero-frequency value of the absorbance. Nearly the same contributions to the prefactor come from the interband dispersion (5/64) in Eq. (16) and the matrix-element variation (4/64) in Eq. (17).

Indeed, in agreement with the analytical results, above $\omega = 0$ the *ab initio* calculated absorbance increases $\sim\omega^2$ as indicated in the inset of Fig. 1. According to the analytical studies, this trend is mainly a consequence of the deviation of the $\pi - \pi^*$ interband energies (13) and dipole matrix elements (15) from the linearity and isotropy of the Dirac particles. The qualitative agreement of the *ab initio* computations (6) in Fig. 2 and tight-binding calculations (7) is underlined by the fit values from the curves in the inset of Fig. 2, $\beta = 0.23$, 0.62, and 0.58 $(\text{eV})^{-1}$ and the values $\beta = 0.10$, 0.23, and 0.30 $(\text{eV})^{-1}$ calculated by the expression (7), but with improved energies (16) and improved matrix elements (17), for graphene, silicene, and germanene, respectively. As a consequence, the quadratic term in the tight-binding result for the low-frequency absorbance (18) underestimates the dispersion deviations from the Dirac cones compared to the *ab initio* results for the absorbance in Fig. 2.

The deviations in the absolute values are mainly a consequence of the neglect of the second- and more distant-neighbor interactions in the tight-binding approach. The deviations from a chemical trend along the row C→Si→Ge of the *ab initio* calculated β values are a consequence of the deviations of the real electronic structure with respect to the Dirac-cone behavior [see Figs. 3(a) and 3(b)]. Figure 1 shows that in germanene the first minimum at Γ appears for lower energies than the saddle point at M, in contrast to silicene and graphene.

F. Region of van Hove singularities

In contrast to the behavior in the infrared spectral region in Fig. 2, the absorbance shows completely different frequency variations for the three 2D honeycomb materials graphene, silicene, and germanene in the visible and ultraviolet spectral regions, as shown in Fig. 5. The main reason is related to the different band structures [see Fig. 3(b)], especially the interband ones in Fig. 1. The van Hove singularities in the

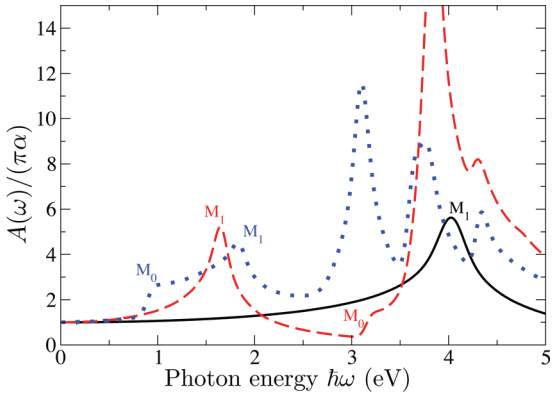

FIG. 5. (Color online) Spectral absorbance (in units of $\pi\alpha$) for graphene (black solid line), silicene (red dashed line), and germanene (blue dotted line).

joint density of states in Fig. 1 and the energy dependence of the optical matrix elements determine the lineshape of the absorbance. The peaks and shoulders in $A(\omega)$ can be almost related to minima (M_0), maxima (M_2) or saddle points (M_1) in the 2D interband band structure and JDOS[47] (as indicated by dotted horizontal lines in Fig. 1), respectively. Because of the strong transition strength at the M point in the 2D BZ [see matrix elements in Fig. 3(a)] the saddle point in the difference $\varepsilon_c(\mathbf{k}) - \varepsilon_v(\mathbf{k})$ of the lowest conduction band (π^*-like) and highest valence band (π-like) gives rise to a pronounced peak at 4.0 eV (graphene), 1.6 eV (silicene), or 1.7 eV (germanene). Of course, the true position should be somewhat shifted to higher energies due to quasiparticle and excitonic effects, e.g., by 0.5 eV as shown for graphene.[8] The other spectral features appearing for silicene and germanene can be also explained in terms of the joint band structure and density of states in Fig. 1. The right-handed step at $\hbar\omega = 0.9$ eV for germanene is in agreement with the 2D nature and the minimum character of the lowest interband transitions at Γ. The absorbance feature near $\hbar\omega = 3.1$ eV is related to manifold contributions from M_0, M_1, and M_2 at the ΓM and MK lines (see Fig. 1), enforced by high JDOS due to several band crossings. The most pronounced structure in the spectrum for silicene at $\hbar\omega = 3.9$ eV is mainly related to the M_2 maximum of the interband transition energy at the ΓM line. However, there are also contributions from M_0 singularities at Γ, M, and K points as well as M_1 on the MK lines. Also the remaining features in the spectra of Fig. 5 can be approximately related to critical points and van Hove singularities in Fig. 1.

G. Gauge invariance of absorbance

The absorbance of the three 2D crystals graphene, silicene, and germanene is displayed in Fig. 6 versus a wide range of photon energies. The two different gauges of the electromagnetic field expressed by the two types of transition matrix elements (2) and (3) have been used. The figure clearly demonstrates that within the used PAW approach the longitudinal and transversal expressions for the frequency-dependent absorbance yield identical results for the energy positions of the spectral features as peaks and shoulders. This is a consequence of the identical joint density of states used. However, also the peak heights are more or less independent of the used description of the transition matrix elements, at least for C- and Ge-based sheets. This fact numerically confirms the assumption that the PAW approach generates all-electron wave functions and eigenvalues for the valence and conduction states.[38] The fictitious all-electron potential is local in space and hence leads to the strict relation between the matrix elements in Eqs. (2) and (3). Only for Si the peak intensities are slightly reduced when the longitudinal expression is applied for $A(\omega)$. The same effect has been observed for the absorption spectra of bulk silicon.[39] The deviation is mainly a consequence of the numerical description. The authors[39] argued that the discrepancies between the two gauges may be compensated by the inclusion of d state projectors and d one-center terms within the PAW spheres.

IV. SUMMARY

Summarizing, we have studied the optical absorbance of the 2D honeycomb crystals graphene, silicene, and germanene by *ab initio* and analytical calculations within the

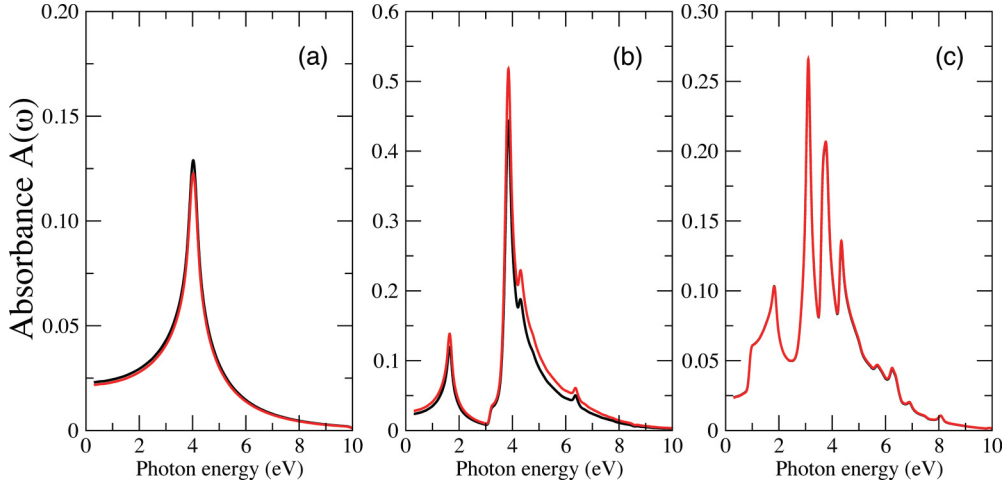

FIG. 6. (Color online) The frequency-dependent absorbance for (a) graphene, (b) silicene, and (c) germanene. Besides the longitudinal gauge (2) (black solid line) also the transversal gauge (3) (red solid line) has been used.

independent-particle approach. We started with the full electronic structure of the sheets as derived within the common Fermi-liquid picture, i.e., with 2D Bloch bands and Bloch wave functions. In the limit of vanishing frequencies, we found $A(0) = \pi\alpha$ as predicted for chiral massless Dirac fermions. This result is explained by an isotropic linear band structure around the six K and K' Dirac points and optical interband matrix elements at these points which can be universally related to the Fermi velocity v_F of the 2D material, i.e., to the slope of the linear bands. This result is independent of the longitudinal or transverse gauge of the electromagnetic field and universal for all group-IV crystals independent of the value of v_F, the degree of sp^2 and sp^3 hybridizations, and the sheet buckling. The lowest optical $\pi - \pi^*$ transitions at K and K' are dipole-allowed. For higher frequencies, the absorbance spectra start to deviate significantly with the group-IV material. We have related this fact mainly to deviations from the Dirac-cone behavior of the interband energies and the corresponding matrix elements for higher photon energies. The low-lying van Hove singularities in the joint density of states are however observable for photon energies in the visible and ultraviolet spectral regions.

ACKNOWLEDGMENTS

We thank R. Del Sole, F. Furthmüller, K. Hannewald, and G. LeLay for valuable scientific discussions. L.M. acknowledges financial support within the EU FP7 Clermont4 project (GA 235114), from Carl-Zeiss Foundation, and from DFG Graduate School 1523 "Quantum and Gravitational Fields." O. P. acknowledges EU FP7 IRSES ROBOCON (GA 230832) for support. P.G. acknowledges FP7 ETSF (GA 211956, user project number 216). CPU time was granted from CINECA and ENEA-CRESCO.

[1] K. S. Novoselov, A. K. Geim, S. V. Morozov, D. Jiang, Y. Zhang, S. V. Dubonos, I. V. Grigorieva, and A. A. Firsov, Science **306**, 666 (2004).
[2] K. S. Novoselov, A. K. Geim, S. V. Morozov, D. Jiang, M. I. Katsnelson, I. V. Grigorieva, S. V. Dubonos, and A. A. Firsov, Nature (London) **438**, 197 (2005).
[3] Y. Zhang, Y.-W. Tan, H. L. Stormer, and P. Kim, Nature (London) **438**, 201 (2005).
[4] T. Ando, Y. Zheng, and H. Suzuura, J. Phys. Soc. Jpn. **71**, 1318 (2002).
[5] V. P. Gusynin and S. G. Sharapov, Phys. Rev. B **73**, 245411 (2006).
[6] R. R. Nair, P. Blake, A. N. Grigorenko, K. S. Novoselov, T. J. Booth, T. Stauber, N. M. R. Peres, and A. K. Geim, Science **320**, 1308 (2008).
[7] K. F. Mak, M. Y. Sfeir, Y. Wu, C. H. Lui, J. A. Misewich, and T. F. Heinz, Phys. Rev. Lett. **101**, 196405 (2008).
[8] L. Yang, J. Deslippe, C.-H. Park, M. L. Cohen, and S. G. Louie, Phys. Rev. Lett. **103**, 186802 (2009).
[9] V. Gusynin, S. Sharapov, and J. Carbotte, Int. J. Mod. Phys. B **21**, 4611 (2007).
[10] T. Stauber, N. M. R. Peres, and A. K. Geim, Phys. Rev. B **78**, 085432 (2008).
[11] M. Lewkowicz and B. Rosenstein, Phys. Rev. Lett. **102**, 106802 (2009).
[12] J. P. Reed, B. Uchoa, Y. I. Joe, Y. Gan, D. Casa, E. Fradkin, and P. Abbamonte, Science **330**, 805 (2010).
[13] S. Cahangirov, M. Topsakal, E. Aktürk, H. Şahin, and S. Ciraci, Phys. Rev. Lett. **102**, 236804 (2009).
[14] A. Grüneis, R. Saito, G. G. Samsonidze, T. Kimura, M. A. Pimenta, A. Jorio, A. G. Souza Filho, G. Dresselhaus, and M. S. Dresselhaus, Phys. Rev. B **67**, 165402 (2003).
[15] P. Gori, O. Pulci, M. Marsili, and F. Bechstedt, Appl. Phys. Lett. **100**, 043110 (2012).
[16] O. Pulci, P. Gori, M. Marsili, V. Garbuio, R. D. Sole, and F. Bechstedt, Europhys. Lett. **98**, 37004 (2012).
[17] P. Vogt, P. De Padova, C. Quaresima, J. Avila, E. Frantzeskakis, M. C. Asensio, A. Resta, B. Ealet, and G. Le Lay, Phys. Rev. Lett. **108**, 155501 (2012).
[18] L. Chen, C.-C. Liu, B. Feng, X. He, P. Cheng, Z. Ding, S. Meng, Y. Yao, and K. Wu, Phys. Rev. Lett. **109**, 056804 (2012).
[19] P. De Padova, C. Quaresima, C. Ottaviani, P. M. Sheverdyaeva, P. Moras, C. Carbone, D. Topwal, B. Olivieri, A. Kara, H. Oughaddou, B. Aufray, and G. Le Lay, Appl. Phys. Lett. **96**, 261905 (2010).
[20] B. Aufray, A. Kara, S. Vizzini, H. Oughaddou, C. Leandri, B. Ealet, and G. L. Lay, Appl. Phys. Lett. **96**, 183102 (2010).
[21] A. Fleurence, R. Friedlein, T. Ozaki, H. Kawai, Y. Wang, and Y. Yamada-Takamura, Phys. Rev. Lett. **108**, 245501 (2012).
[22] F. Bechstedt, L. Matthes, P. Gori, and O. Pulci, Appl. Phys. Lett. **100**, 261906 (2012).
[23] I. Sodemann and M. M. Fogler, Phys. Rev. B **86**, 115408 (2012).
[24] P. Hohenberg and W. Kohn, Phys. Rev. **136**, B864 (1964).
[25] W. Kohn and L. J. Sham, Phys. Rev. **140**, A1133 (1965).
[26] G. Kresse and J. Furthmüller, Phys. Rev. B **54**, 11169 (1996).
[27] G. Kresse and J. Furthmüller, Comput. Mater. Sci. **6**, 15 (1996).
[28] J. Perdew, in *Electronic Structure of Solids '91* (Akademie-Verlag, Berlin, 1991).
[29] J. P. Perdew and Y. Wang, Phys. Rev. B **45**, 13244 (1992).
[30] P. E. Blöchl, Phys. Rev. B **50**, 17953 (1994).
[31] G. Kresse and D. Joubert, Phys. Rev. B **59**, 1758 (1999).
[32] H. J. Monkhorst and J. D. Pack, Phys. Rev. B **13**, 5188 (1976).
[33] B. Uchoa, J. P. Reed, Y. Gan, Y. I. Joe, E. Fradkin, P. Abbamonte, and D. Casa, Phys. Scr. **2012**, 014014 (2012).
[34] C.-C. Liu, W. Feng, and Y. Yao, Phys. Rev. Lett. **107**, 076802 (2011).
[35] A. Bostwick, F. Speck, T. Seyller, K. Horn, M. Polini, R. Asgari, A. H. MacDonald, and E. Rotenberg, Science **328**, 999 (2010).
[36] A. Schleife, C. Rödl, F. Fuchs, K. Hannewald, and F. Bechstedt, Phys. Rev. Lett. **107**, 236405 (2011).
[37] K. F. Mak, L. Ju, F. Wang, and T. F. Heinz, Solid State Commun. **152**, 1341 (2012).
[38] B. Adolph, J. Furthmüller, and F. Bechstedt, Phys. Rev. B **63**, 125108 (2001).
[39] M. Gajdoš, K. Hummer, G. Kresse, J. Furthmüller, and F. Bechstedt, Phys. Rev. B **73**, 045112 (2006).

[40]S. Lebègue, M. Klintenberg, O. Eriksson, and M. I. Katsnelson, Phys. Rev. B **79**, 245117 (2009).
[41]S. Lebègue and O. Eriksson, Phys. Rev. B **79**, 115409 (2009).
[42]L. C. Lew Yan Voon, E. Sandberg, R. S. Aga, and A. A. Farajian, Appl. Phys. Lett. **97**, 163114 (2010).
[43]T. H. Osborn, A. A. Farajian, O. V. Pupysheva, R. S. Aga, and L. L. Y. Voon, Chem. Phys. Lett. **511**, 101 (2011).
[44]G. G. Guzmán-Verri and L. C. Lew Yan Voon, Phys. Rev. B **76**, 075131 (2007).
[45]P. Yu and M. Cardona, in *Fundamentals of Semiconductors* (Springer, Berlin, 1996).
[46]A. H. Castro Neto, F. Guinea, N. M. R. Peres, K. S. Novoselov, and A. K. Geim, Rev. Mod. Phys. **81**, 109 (2009).
[47]G. Grosso and G. Pastori Parravicini, in *Solid State Physics* (Academic Press, Cambridge, 2003).